

Phenotypic Discovery of SB1501, an Anti-obesity Agent, through Modulating Mitochondrial Activity

Ala Jo⁺,^[a] Mingi Kim⁺,^[a] Jong In Kim,^[b] Jaeyoung Ha,^[c] Yoon Soo Hwang,^[a] Hyunsung Nam,^[a] Injae Hwang,^[b] Jae Bum Kim,^[b] and Seung Bum Park*^[a, c]

Obesity has become a pandemic that threatens the quality of life and discovering novel therapeutic agents that can reverse obesity and obesity-related metabolic disorders are necessary. Here, we aimed to identify new anti-obesity agents using a phenotype-based approach. We performed image-based high-content screening with a fluorogenic bioprobe (SF44), which visualizes cellular lipid droplets (LDs), to identify initial hit compounds. A structure-activity relationship study led us to yield a bioactive compound SB1501, which reduces cellular LDs in 3T3-L1 adipocytes without cytotoxicity. SB1501 induced the

expression of gene products that regulate mitochondrial biogenesis and fatty acid oxidation in 3T3-L1 adipocytes. Daily treatment with SB1501 improved the metabolic states of *db/db* mice by reducing body fat mass, adipose tissue mass, food intake, and increasing glucose tolerance. The anti-obesity effect of SB1501 may result from perturbation of the PGC-1 α -UCP1 regulatory axis in inguinal white adipose tissue and brown adipose tissue. These data suggest the therapeutic potential of SB1501 as an anti-obesity agent via modulating mitochondrial activities.

Introduction

In recent decades, obesity has become a pandemic that threatens the quality of life. Obesity is positively associated with the risk of metabolic diseases, such as type 2 diabetes, dyslipidemia, hypertension, cardiovascular diseases, and various cancers.^[1–4] Currently, over one-third of adults worldwide are obese, and the rate of obesity has doubled in 73 countries since 1980.^[5] The consistent increase in the obese population constitutes an enormous medical and social burden in the 21st century. Thus, the demand for novel therapeutic agents that can reverse obesity and obesity-related metabolic disorders continues to grow.

At present, five drugs have been approved by the U.S. Food and Drug Administration (FDA) as anti-obesity agents in patients with a body mass index (BMI) ≥ 27 kg/m² and at least one obesity-related metabolic disorder or patients with BMI ≥ 30 kg/m².^[6,7] These drugs focus primarily on reducing energy intake by targeting pathways in the central nervous system (CNS) or preventing dietary fat absorption by inhibiting gastric and pancreatic lipases in the case of orlistat.^[8] Still, they pose

safety concerns due to unwanted adverse effects.^[9,10] As an alternative approach, small-molecule mitochondrial uncouplers have gained attention as anti-obesity agents. Mitochondrial uncouplers show significant weight-loss effects by allowing protons to enter the mitochondrial matrix without generating ATP, thereby increasing the oxidation of circulating lipids and the cellular glucose uptake to compensate for the total amount of ATP.^[11] These observations highlight mitochondrial uncouplers as attractive therapeutic agents for reversing obesity. Even though certain molecules might be specific to mitochondria, only a few have anti-obesity effects with a suitable therapeutic window.^[12] For example, the small molecule 2,4-dinitrophenol is the best-studied uncoupler, but its clinical use was banned due to toxicity issues.^[13] Therefore, there remains a need for new chemical entities (NCEs) that present therapeutic potential as anti-obesity agents with improved safety profiles.

This study aims to discover new anti-obesity agents using a phenotype-based approach, which focuses on phenotypic changes in cells or organisms as an outcome of perturbation in multiple interconnected pathways.^[14] This approach can be more powerful when diseases have high biological heterogeneity or their therapeutic targets are not thoroughly defined. Thus, phenotype-based drug discovery has emerged as a promising approach for identifying NCEs as candidates for first-in-class drugs.^[15]

Here, we performed an image-based high-content screening for quantitative monitoring of cellular lipid droplets (LDs) with a fluorogenic LD bioprobe (SF44).^[16] We discovered a new bioactive compound, SB1501, which contains a benzopyran-substituted 1,2,3-triazole as a new small-molecule that reduces cellular LD accumulation. We demonstrated that SB1501 significantly reduces cellular LDs in 3T3-L1 adipocytes differentiated from murine embryonic fibroblast and HeLa human cervical cancer cells. We also observed the reduction of fat accumulation in adipose tissues and body weight along with

[a] Dr. A. Jo,⁺ M. Kim,⁺ Y. S. Hwang, H. Nam, Prof. S. B. Park
CRI Center for Chemical Proteomics
Department of Chemistry, Seoul National University
Seoul 08826 (Korea)
E-mail: sbpark@snu.ac.kr

[b] Dr. J. I. Kim, Dr. I. Hwang, Dr. J. B. Kim
CRI Center for Adipocyte Structure–Function
School of Biological Sciences, Seoul National University
Seoul 08826 (Korea)

[c] J. Ha, Prof. S. B. Park
Department of Biophysics and Chemical Biology
Seoul National University
Seoul 08826 (Korea)

[†] These authors contributed equally to this work.

Supporting information for this article is available on the WWW under <https://doi.org/10.1002/cmdc.202100062>

improved glucose tolerance in a *db/db* mouse model. We further demonstrated that SB1501 might manifest its anti-obesity effect by perturbing the PGC-1 α -UCP1 regulatory axis. In summary, we identified the therapeutic potential of SB1501 as an anti-obesity agent.

Results and Discussion

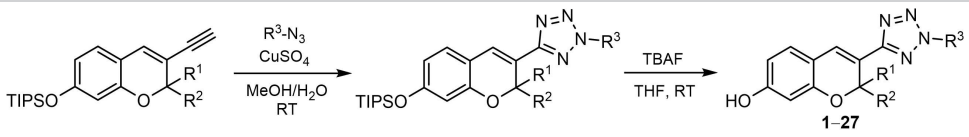
Discovery of SB1501 and its structure–activity relationship study

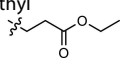
Obesity is a metabolic condition involving excess fat accumulation in adipose tissues. Under obesity, adipocytes store excessive energy in the form of triglycerides in LDs, resulting in an expansion of cell sizes.^[17] One of the most significant phenotypic changes in adipocytes under obesity is the enlargement of cellular LDs caused by fat accumulation.^[18] As we envisioned the phenotype-based discovery of novel small-molecule modulators that reduce cellular fat accumulation, we first established cell-based high-throughput phenotypic screening with the fluorogenic LD-staining dye (SF44) for quantitative monitoring of cellular LDs and lipid metabolism in HeLa cells.^[19]

Using SF44 that turns on in the hydrophobic environment of LDs, we robustly monitored the homeostasis of cellular LDs in live cells without any fixation or washing steps (Figure S1 in the Supporting Information). These distinct advantages of SF44 allowed the non-invasive measurement of LD homeostasis with excellent practicality compared to other commercial LD probes. We then performed this high-content screening against an approximately 3000-member in-house drug-like poly-heterocycle library constructed using a privileged substructure-based diversity-oriented synthesis (pDOS) strategy.^[20] Our image-based screening resulted in the discovery of the initial hit compound **8** containing a benzopyranyl 1,2,3-triazole skeleton, which reduced cellular LDs down to 67% in HeLa cells at the 10 μ M concentration compared to DMSO-treated cells without significant toxicity (Figure 1a, b and Table 1).

Next, we pursued a structure-activity relationship (SAR) study of our initial hit compound **8** by designing and synthesizing approximately 30 analogs based on the benzopyranyl 1,2,3-triazole scaffold (Figure 1c). We systematically introduced the R¹, R², and R³ substituents on the benzopyranyl 1,2,3-triazole core skeleton (Table 1). We first introduced various aliphatic and aromatic substituents via the copper-mediated click reaction to explore the substituent effects at the R³ group on

Table 1. Structure–activity relationship study of benzopyranyl 1,4-disubstituted-1,2,3-triazole analogs by measuring lipid droplet (LD) organelle count with SF44 and cell viability in HeLa human cervical cancer cells.



Cmpd	R ¹	R ²	R ³	LD count ^[a] [%]	Cell viab. ^[b] [%]
1	methyl	methyl	<i>n</i> -heptyl	121	121
2	methyl	methyl	cyclohexyl	86	101
3	methyl	methyl	cyclohexylmethyl	87	113
4	methyl	methyl	benzyl	106	112
5	methyl	methyl	2-phenylethyl	97	115
6	methyl	methyl	3-pyridyl	119	99
7	methyl	methyl	phenyl	90	110
8	methyl	methyl	4-methoxyphenyl	67 (14) ^[d]	96 (92) ^[e]
9	methyl	methyl	4-trifluoromethylphenyl	103	97
10	methyl	methyl	4-cyanophenyl	96	95
11	methyl	methyl	4-bromophenyl	101	115
12 ^[c]	methyl	methyl	2-methoxyphenyl	47 (8) ^[d]	106 (106) ^[e]
13	methyl	methyl	2-trifluoromethylphenyl	110	115
14	methyl	methyl	2-cyanophenyl	107	95
15	methyl	methyl	2-chlorophenyl	110	98
16	methyl	methyl	3-methoxyphenyl	83	87
17	methyl	methyl	3-trifluoromethylphenyl	97	98
18	methyl	methyl	3-cyanophenyl	90	90
19	methyl	methyl	3-fluorophenyl	129	97
20	methyl	methyl	2-hydroxyphenyl	71 (17) ^[d]	111 (103) ^[e]
21	methyl	methyl	2-aminophenyl	66 (11) ^[d]	103 (99) ^[e]
22	methyl	methyl	2-(<i>N</i> -methyl)aminophenyl	115	102
23	methyl	methyl	2-(<i>N,N</i> -dimethyl)aminophenyl	116	107
24	methyl	methyl	2-nitrophenyl	82	107
25	methyl	methyl	2,5-dimethoxyphenyl	52 (15) ^[d]	101 (110) ^[e]
26	methyl		2-methoxyphenyl	77	110
27	fluoromethyl	fluoromethyl	2-methoxyphenyl	103	103

[a] Lipid droplet organelle count [%] of each compound (10 μ M) was monitored by image-based high throughput assay in HeLa human cervical cancer cells for 1 day. [b] Cell viability assay of each compound (10 μ M) in HeLa cells for 1 day. [c] SB1501. [d] Lipid droplet organelle count [%] of each compound (40 μ M). [e] Cell viability assay of each compound (40 μ M) in HeLa cells for 1 day.

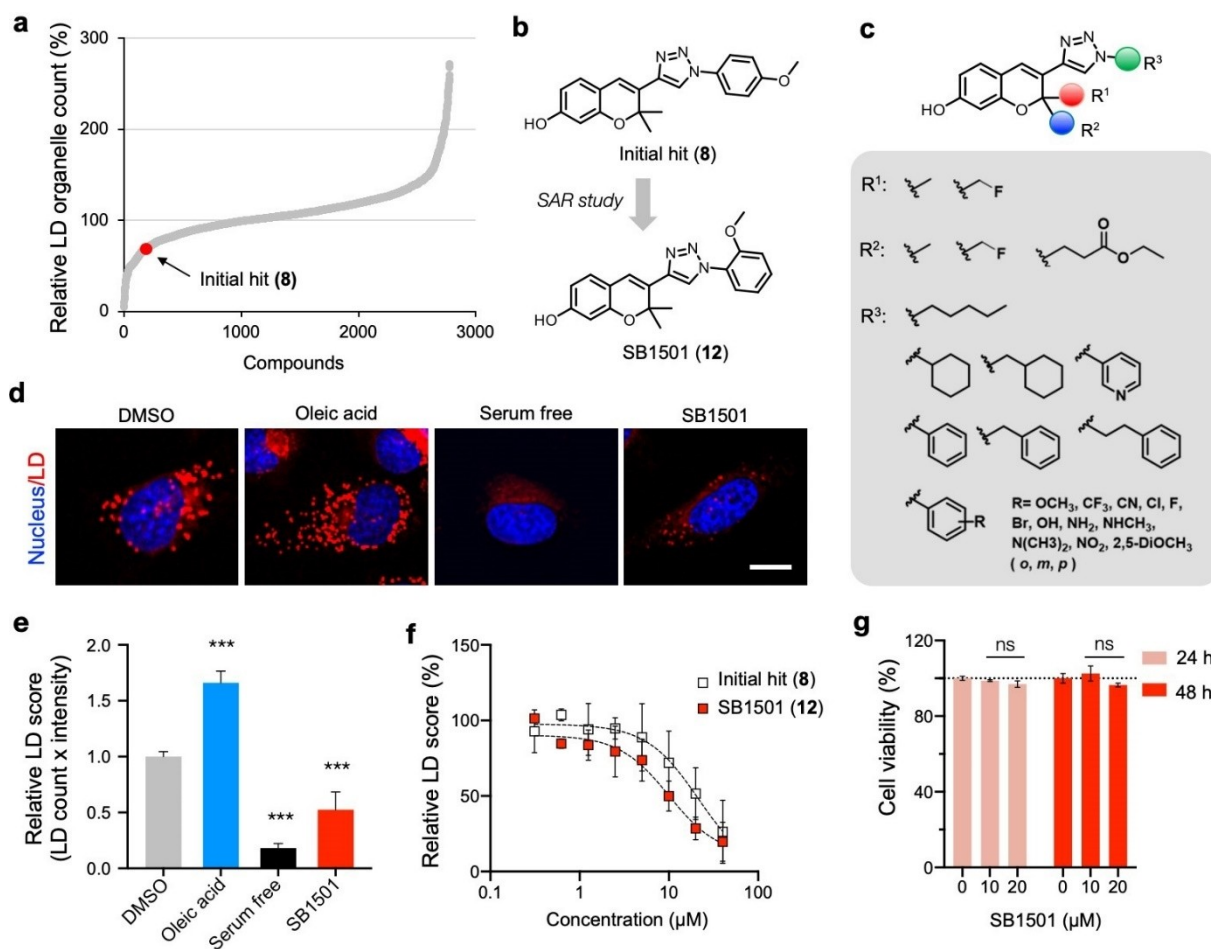


Figure 1. Discovery of SB1501 from phenotypic screening. a) Image-based high-throughput screening against an in-house compound library. Lipid droplet (LD) organelle count [%] of all compounds (10 μ M for 24 h) was monitored in HeLa cells. Data were normalized to a DMSO control. Initial hit compound **8** reduced cellular LDs down to 67% compared to what was found in DMSO-treated cells without significant cytotoxicity. b) Structure of initial hit **8** and SB1501 (**12**). c) Structural modifications of benzopyranyl 1,4-disubstituted-1,2,3-triazoles. R¹ = methyl, fluoromethyl; R² = methyl, fluoromethyl, ester group; R³ = *n*-heptyl, cyclohexyl, cyclohexylmethyl, benzyl, 2-phenylethyl, 3-pyridyl, phenyl, and phenyl with various functional groups. d) Monitoring cellular LDs by fluorescence microscopy. Cellular LDs and nuclei were stained with SF44 and Hoechst 33342, respectively, after treatment with DMSO, oleic acid (5 μ M), serum-free medium (starvation) or SB1501 (10 μ M) for 24 h in HeLa cells. Scale bar: 5 μ m. e) Quantification of cellular LDs from the images in (d). The scores were determined by multiplying the number of LD per cell and mean LD intensity. Each value was normalized to the DMSO control. f) Determination of the EC₅₀ values of initial hit **8** and SB1501 (**12**) in HeLa cells after treatment for 24 h. g) Cytotoxicity of SB1501 in HeLa cells. A cell viability assay was performed after SB1501 treatment for 24 and 48 h. All data are presented as mean \pm SD; ****p* < 0.001 followed by one-way Dunnett's test.

the 1,2,3-triazole ring. Analogs bearing alkyl moieties, such as *n*-heptyl, cyclohexyl, cyclohexylmethyl, benzyl, and 2-phenylethyl groups (1–5), at the R³ position did not show any significant LD reducing activity. Then, we introduced (hetero)aryl groups (7–11) at the R³ position, especially aryl moieties containing various substituents, such as CF₃, CN, and halogen, at the *para* position of the phenyl ring to examine the importance of substituents. Still, we did not find any analogs with higher potency than 4-methoxyphenyl compound **8**. Therefore, we examined these substituents' positional effects by synthesizing a series of analogs (12–18) with all possible positional isomers (*ortho* and *meta*). Independent of the position, we did not observe a cellular LD reduction in analogs possessing electron-withdrawing groups. To our pleasant surprise, compound **12** containing an electron-donating methoxy substituent at the *ortho* position of the phenyl group showed the best efficacy by reducing LDs

by 47% in HeLa cells at 10 μ M (Figure 1b, d and e). Furthermore, the incorporation of hydroxy (**20**) and amino groups (**21**) at the *ortho* position of the phenyl and 2,5-dimethoxy phenyl moieties (**25**) at the R³ position also showed reductions in cellular LDs, but these compounds did not show higher efficacy than compound **12**. Also, under a higher concentration (40 μ M), compound **12** displayed the most drastic reduction in LD organelle count (8%) without cytotoxicity, while compounds **20**, **21**, and **23** showed 17, 15, and 11% reductions, respectively (Table 1).

Keeping the 2-methoxyphenyl group at the R³ position, we modified the substituents of compound **12** at the R¹ and R² positions by introducing a functional handle (**26**) and fluoromethyl group (**27**), but we observed no significant LD-reducing activities. Lastly, the bioisosteric replacement of triazole with isoxazole in the core skeleton was performed, but

the resulting compound (**28**) showed significant cytotoxicity (Figure S2).

To sum up, our image-based high-throughput screening identified the initial hit compound **8** containing benzopyranyl 1,2,3-triazole skeleton, which reduced the cellular LDs in HeLa cells without significant cytotoxicity. Based on our SAR study of initial hit compound **8**, we discovered that the lead compound **12** containing *ortho*-positioned methoxy group on the phenyl ring at the R³ position, dimethyl groups at the R¹ and R² position on benzopyran, and triazole branch between two moieties, showed the best efficacy in the cellular LD reduction. Compound **12** efficiently reduced cellular LDs in a dose-dependent manner in HeLa cells and showed the improved half-maximal effective concentration (EC₅₀) of 10.02 μM (24 h) compared to that of initial hit compound **8** without significant cytotoxicity in HeLa cells for 24 h and 48 h (Figure 1f, g). Therefore, we named this lead compound **12** as SB1501 and pursued its further biological evaluations.

SB1501 reduces fat accumulation in 3T3-L1 adipocytes

We evaluated the LD-reducing activity of SB1501 in differentiating 3T3-L1 adipocytes. 3T3-L1 adipocytes originated from embryonic mouse fibroblasts are widely used to study mature adipocytes *in vitro*.^[21] Upon induction of differentiation, 3T3-L1 preadipocytes start to express the transcriptional regulators of adipogenesis, which results in significant LD maturation via the accumulation of excess fat into LDs (Figure 2a).^[22] As an excessive fat accumulation within adipocyte's LDs is closely associated with pathological conditions of obesity and obesity-related metabolic diseases, targeting the adiposity of adipocytes has been considered as a promising therapeutic approach. To determine whether SB1501 can reduce fat accumulation in 3T3-L1 adipocytes, we treated 3T3-L1 adipocytes with SB1501 along the differentiation process and monitored the subsequent phenotypic changes. Under the continuous exposure of SB1501 to the differentiating 3T3-L1 adipocytes for 8 days, 3T3-L1 adipocytes displayed a significant reduction of cellular fat accumulation at day 8 monitored by Oil Red O staining (Figure 2b), which was confirmed by the biochemical quantification of cellular triglycerides (TGs; Figure S3a). Besides, SB1501 reduced the mRNA and the protein expression level of peroxisome proliferator-activated receptor-gamma (PPAR γ), regulating adipogenesis and lipogenesis (Figure S4a, b). As it has been known that the inhibition of adipogenesis reduces fat accumulation in adipocytes, we examined whether SB1501 inhibits the onset of differentiation at the induction stage of differentiation.^[23,24] When we treated SB1501 for 2 days at the early stage of differentiation (day 0–day 2), we didn't observe the reduction in fat accumulation in 3T3-L1 adipocytes (Figure 2b). Moreover, SB1501 showed LD-reducing effects in differentiated C2 C12 skeletal muscle cell line (Figure S4c). These data imply that SB1501 may not perturb the onset of crucial transcriptional regulators at the early stage of 3T3-L1 adipocyte differentiation. Instead, SB1501 affects fat accumulation and LD maturation in adipocytes.

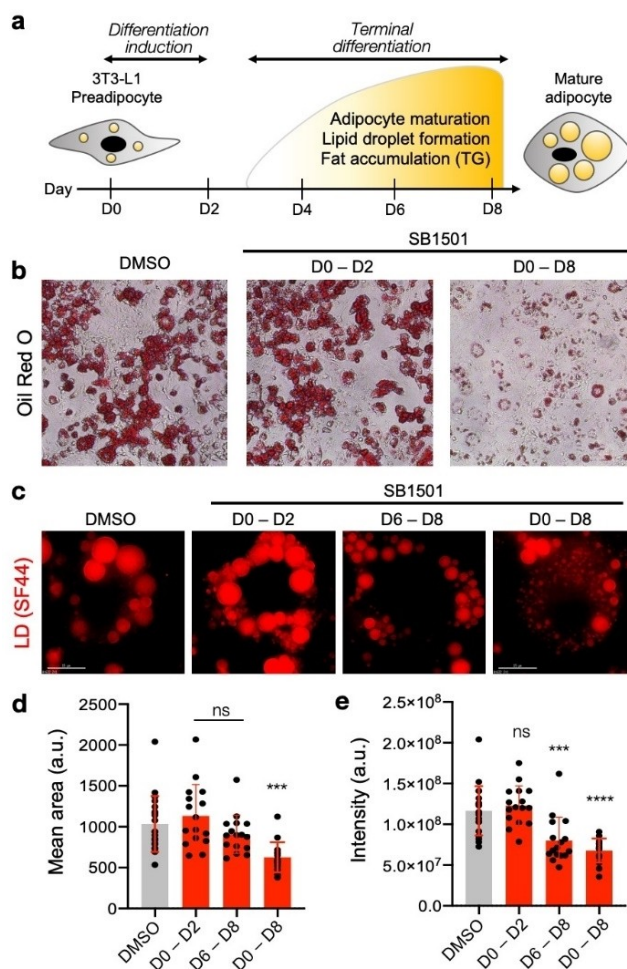


Figure 2. SB1501 reduces the size and fat accumulation of LDs in 3T3-L1 adipocytes. a) Schematic diagram of the 3T3-L1 differentiation process. b) Monitoring of fat accumulation within 3T3-L1 adipocytes after treatment of differentiating cells with SB1501 (40 μM) for 2 days (D0–D2) or 8 days (D0–D8). Oil Red O staining was performed on day 8. c) Representative fluorescence images of 3T3-L1 adipocytes stained with SF44. Cells were treated with SB1501 (40 μM) for different durations after the induction of differentiation. D0–D2; 2-day treatment at the early stage of differentiation, D6–D8; 2-day treatment at the late stage of differentiation, D0–D8; 8-day treatment along the whole differentiation. The fluorescence images were taken on day 8 after staining LDs with SF44. Scale bars: 15 μm. Quantification of the d) mean area and e) fluorescence intensities of LDs from the images in (c). Each dot represents a single cell. All data are presented as mean ± SD; ****p* < 0.001 followed by one-way Dunnett's test. ns, not statistically significant.

To investigate its underlying mechanism of action, we treated SB1501 at different treatment times after the induction of differentiation. We observed phenotypic changes in differentiating 3T3-L1 adipocytes by monitoring cellular LDs with live-cell fluorescent microscopy after SF44 staining (Figure S3b). Upon long-term treatment of SB1501 (days 0–8), differentiated 3T3-L1 adipocytes showed a significant reduction in the size of multilocular LDs, compared to DMSO-treated cells as a negative control (Figure 2c). Quantitative image analysis further revealed that the size of every single LD and the fat accumulation within LDs were reduced upon 8-day treatment with SB1501 (Fig-

ure 2d, e). In contrast, short-term 2-day treatment of SB1501 at the early stage of differentiation (day 0 to day 2) did not display significant changes in the phenotype of LDs. In contrast, cells treated with SB1501 at the late stage of differentiation for 2 days (day 6 to day 8) showed more efficient LD-reducing effects (Figure 2c–e). Moreover, the LD-reducing effects of SB1501 showed a positive correlation with the duration of SB1501 treatment (Figure S3c, d). Collectively, our phenotypic observation suggested that SB1501 would reduce the size of LDs and fat accumulation via the perturbation of lipid metabolism in mature adipocytes.

Mechanism of action study of SB1501

LDs are vital subcellular organelles that regulate lipid metabolism in response to cellular energy demands. LD size and its energy storage capacity are tightly controlled by the balance among lipogenesis, lipolysis, and fatty acid oxidation (FAO) (Figure 3a).^[25,26] Excessive energy sources are transformed into TGs and transferred into LDs by lipogenesis. Under energy-deficient conditions, lipolysis facilitates the hydrolysis of TGs into free fatty acids and glycerol, and fatty acids (FAs) released from LDs are utilized in mitochondrial FAO for ATP generation.^[27] In fact, both pathways have been considered as therapeutic targets to overcome obesity and obesity-related metabolic diseases.

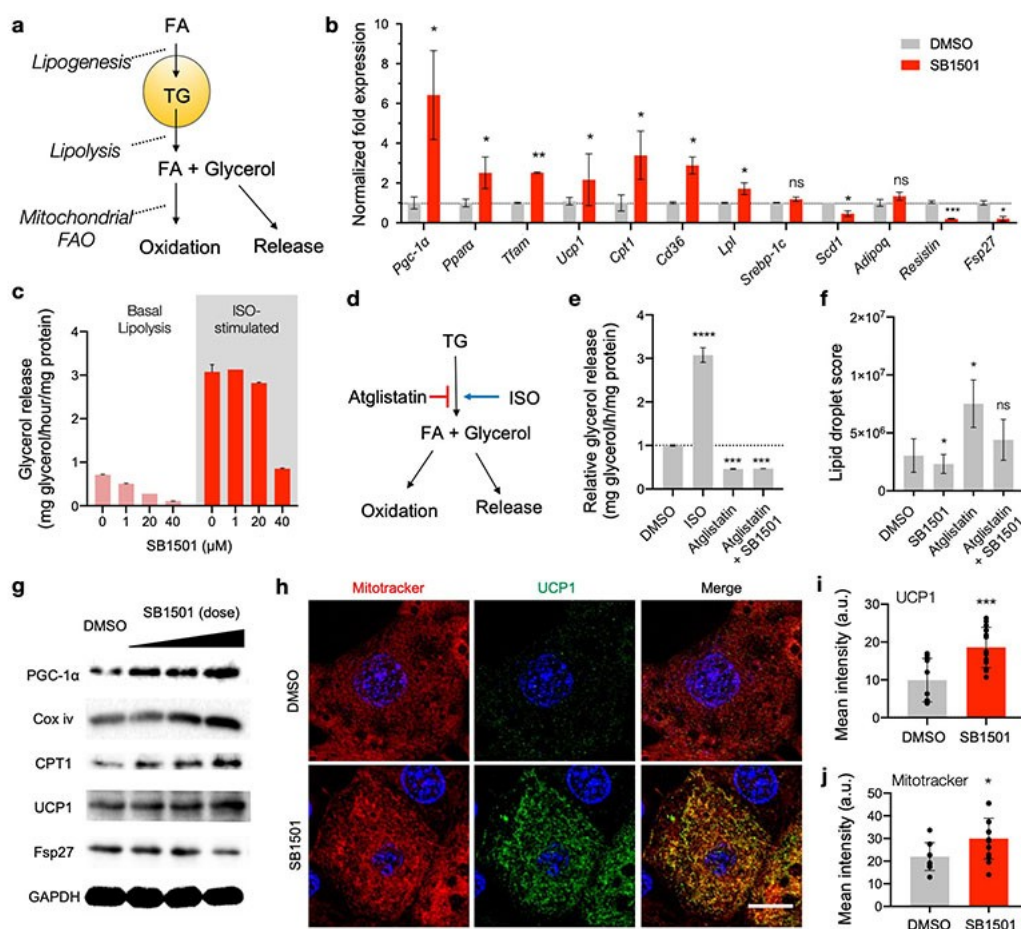


Figure 3. Mechanism of action study of SB1501 in 3T3-L1 adipocytes. a) Schematic diagram of cellular LD regulation by lipogenesis, lipolysis, and mitochondrial fatty acid oxidation (FAO). b) Quantitative analysis of mRNA expression in 3T3-L1 adipocytes. qRT-PCR was performed after 3T3-L1 adipocytes were treated with SB1501 (40 μM) for 8 days. Fold expressions of each gene were normalized to DMSO control. c) Lipolysis assay in 3T3-L1 adipocytes upon SB1501 treatment. Differentiating 3T3-L1 adipocytes were treated with SB1501 (40 μM) for 8 days. Glycerol release was measured by using a lipolysis assay kit at day 8 with or without isoproterenol (ISO) stimulation (100 nM). d) Schematic diagram of lipolysis and its modulation with lipolysis inducer (ISO) and inhibitor (atglistatin). ISO induces lipolysis thereby increasing glycerol release. Atglistatin reduces glycerol release by inhibiting the activity of lipase. e) Monitoring glycerol release in 3T3-L1 adipocytes after treatment with ISO (100 nM, 2 h), atglistatin (1 μM, 6 h), or co-treatment of atglistatin with SB1501 (40 μM, 6 h). f) Effect of SB1501 and atglistatin on cellular LD accumulation. LDs of 3T3-L1 preadipocytes were monitored after treatment with SB1501 (20 μM), atglistatin (100 nM), or co-treatment of atglistatin with SB1501 for 24 h. g) Western blot images of PGC-1α and proteins that regulate mitochondrial biogenesis and the FAO pathway. Differentiating 3T3-L1 adipocytes were treated with SB1501 (40 μM) for 8 days. h) Representative immunofluorescence images of 3T3-L1 adipocytes stained with UCP1 (green) and MitoTracker Red (red). Scale bar: 15 μm. Quantified fluorescence intensity of i) UCP1 and j) MitoTracker Red from the imaged in (h). Each dot represents a single cell. All data are presented as mean ± SD; **p* < 0.05, ***p* < 0.01, ****p* < 0.001, *****p* < 0.0001 followed by unpaired Student's *t*-test (b, i, j) and one-way Dunnett's test (e, f). ns: not statistically significant.

To understand the mechanism of action underlying the LD-reducing effect of SB1501, we examined whether SB1501 influences the expression levels of regulatory genes for lipid metabolism in differentiating 3T3-L1 adipocytes. We first examined the mRNA expression level of peroxisome proliferator-activated receptor- γ coactivator-1- α (PGC-1 α) and its downstream proteins involved in mitochondria biogenesis and FAO. PGC-1 α is a transcriptional co-activator and one of the main regulators of energy metabolism in mammalian cells.^[28] PGC-1 α regulates metabolic signaling pathways, including adaptive thermogenesis, mitochondria biogenesis, and FAO.^[29–32] As shown in Figure 3b, we observed the elevated mRNA levels of regulatory proteins for mitochondrial biogenesis (PGC-1 α , PPAR α , and TFAM) and FAO (UCP1, CPT1, CD36, and LPL), compared to those of DMSO-treated cells. The mRNA level of Fsp27 was also reduced, which mediates the fusion of cellular LDs in response to increased cellular lipid accumulation.^[33] SB1501 significantly suppressed the mRNA level of resistin, an adipokine known to promote obesity-related insulin resistance.^[34] In contrast, the mRNA level of adiponectin (AdipoQ), which enhances insulin sensitivity,^[35] was not significantly changed. Meanwhile, the mRNA level of SREBP-1, a transcription factor that facilitates lipogenesis, showed little difference compared to DMSO-treated cells, but the mRNA level of SCD1 was somewhat decreased.

Next, to investigate whether SB1501 induces lipolysis, we performed a lipolysis assay in 3T3-L1 adipocytes.^[36] Since the pharmacological induction of lipolysis results in the breakdown of TGs into FAs and the decrease of TG accumulation within LDs, a direct effect on adipocyte lipolysis could be of therapeutic interest for reducing obesity and improving insulin resistance.^[37–39] Therefore, we hypothesized that SB1501 might increase the release of glycerol by inducing lipolysis similar to the effect of isoproterenol (ISO), a β -adrenergic receptor agonist that activates hormone-sensitive lipases (Figure 3d).^[40] The treatment of differentiated 3T3-L1 adipocytes with ISO (100 nM) drastically enhanced the released amount of glycerol, compared to the DMSO-treated group (basal lipolysis, Figure 3c). However, the SB1501-treated group showed a reduction in the glycerol release in a dose-dependent manner with or without ISO stimulation (Figure 3c). In contrast, atglistatin, a lipolysis inhibitor that blocks TG degradation,^[41] reduced the glycerol release in differentiated 3T3-L1 adipocytes while significantly elevating the cellular LD accumulation (Figure 3e, f). Besides, the co-treatment of atglistatin with SB1501 reversed the fat-accumulating effect of atglistatin (Figure 3f and S5). These data showed that SB1501 reduces the cellular LD accumulation via a distinct mechanism of action different from lipolysis inducer (ISO) and inhibitor (atglistatin).

Next, we further investigated whether SB1501 perturbs the expression of regulatory proteins for mitochondrial biogenesis and FAO. Several studies have revealed that the induction of mitochondrial biogenesis and FAO can reverse fat accumulation, which may contribute to overcoming obesity-related metabolic disorders.^[42–44] Based on our mRNA level analysis, we examined the protein expression of PGC-1 α and its downstream proteins involved in mitochondria biogenesis and FAO. Western

blot analysis revealed that the 8-day treatment of SB1501 increased the protein levels of PGC-1 α , COX IV, and CPT1 in 3T3-L1 adipocytes (Figure 3g). In contrast, SB1501 reduced the protein levels of fat-specific protein 27 (FSP27) in a dose-dependent manner consistent with inhibition at the mRNA level. Notably, the expression of mitochondrial uncoupling protein 1 (UCP1) was upregulated upon SB1501 treatment in a dose-dependent manner as a downstream effect of PGC-1 α upregulation (Figure 3g). UCP1, a downstream protein of PGC-1 α , is the gold standard protein marker for adaptive thermogenesis in adipocytes.^[45,46] UCP1 is localized in the inner mitochondrial membrane and functions to uncouple oxidative phosphorylation. The induction of UCP1 increases cellular energy expenditure by dissipating fatty acids as heat, which leads to reduced fat accumulation.^[47] Consistent with the data above, immunofluorescence analysis further demonstrated the upregulation of UCP1 along with its co-localization of MitoTracker upon SB1501 treatment (Figure 3h–j). Together, these data suggest that SB1501 increases mitochondrial biogenesis and FAO with upregulation of PGC-1 α -UCP1 regulatory axis, which leads to reduced fat accumulation and demand for lipid storage capacity in 3T3-L1 adipocyte.

SB1501 improves mitochondrial function

We then investigated the correlation between the LD-reducing activity of SB1501 and mitochondrial morphology in 3T3-L1 adipocytes. Cellular energy expenditure is closely linked to the regulation of mitochondria fusion and fission dynamics.^[48] Especially, *in vitro* studies with 3T3-L1 cells revealed the correlation between TG accumulation and mitochondrial dynamics.^[49,50] PGC-1 α is known to regulate both mitochondrial biogenesis and morphology along with its downstream regulators. To investigate whether SB1501 perturbs mitochondrial morphology through PGC-1 α upregulation, we examined the architectural changes of mitochondria in differentiated 3T3-L1 adipocytes upon treatment with SB1501 via live-cell imaging. As shown in Figure 4a, high-resolution imaging of mitochondria and LDs in live cells showed a significant increase in mitochondria fusion along with the decreased LD accumulation upon 8-day treatment of SB1501. Quantitative analysis of images revealed that the average volume of the mitochondrial network was increased in SB1501-treated cells, compared to the DMSO-treated cells, while the number of mitochondrial networks per cell remained the same (Figure 4b, c). SB1501 also increased mitochondrial fusion in a time-dependent manner in 3T3-L1 adipocytes (Figure S6) as well as in HeLa cells (Figure S7), which is consistent with its LD-reducing effect.

We then performed bioenergetic studies using a Seahorse XF Analyzer to assess the effect of SB1501 on mitochondrial function in differentiating 3T3-L1 adipocytes. Upon 8-day treatment of SB1501, we observed a significant increase in the maximal mitochondrial respiration compared to the DMSO-treated cells, in accordance with elevated oxygen consumption rate by upregulated level of UCP1 (Figure 4d).^[51–53] In addition, the copy number of mitochondrial DNA (mtDNA) was increased

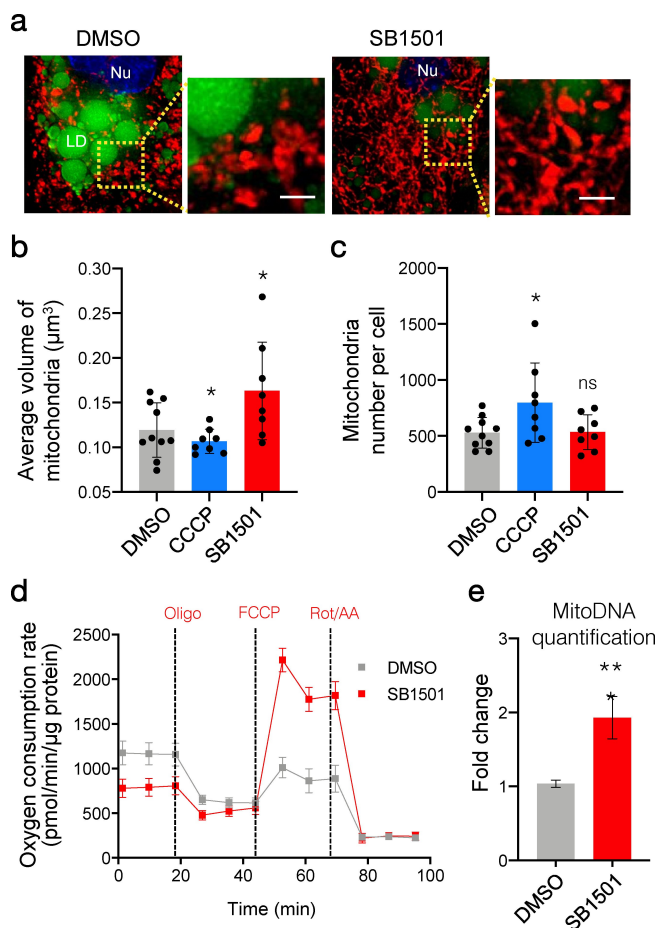


Figure 4. Cellular effects of SB1501 on mitochondrial function and morphology. a) Representative fluorescence images of 3T3-L1 adipocytes stained with SF44 for LDs (green) and MitoTracker Red for mitochondria (red) upon treatment with SB1501 (40 μ M) for 8 days. Scale bars: 2 μ m. Quantification of b) average volume and c) number of mitochondrial networks per cell from the images in (a). Each dot represents a single cell. d) Measurement of oxygen consumption rate (OCR) by using Seahorse XFe24 Analyzer [Seahorse Bioscience] in 3T3-L1 adipocytes after treatment of differentiating 3T3-L1 cells with SB1501 (40 μ M) or DMSO for 8 days. $N=7$ for each group. e) Quantification of mitochondrial DNA (MitoDNA) in 3T3-L1 adipocytes treated with SB1501 (40 μ M) for 8 days. All data are presented as mean \pm SD. $n=3$ biologically independent experiments. * $p < 0.05$, *** $p < 0.001$ followed by one-way Dunnett's test (b,c) or unpaired Student's t -test (d,e,f). ns: not statistically significant.

by 1.9-fold ($p=0.0009$), which further suggested that SB1501 induces mitochondrial biogenesis (Figure 4e). These observations suggest that SB1501 would increase the cellular energy expenditure of adipocytes by elevating mitochondrial biogenesis and perturbing mitochondrial dynamics.

Anti-obesity effects of SB1501 in a *db/db* mouse model

Next, we investigated whether SB1501 shows anti-obesity effects *in vivo*. When we first performed a pharmacokinetic study to decide the administration route, oral administration of SB1501 (10 mg/kg) showed 42.9% oral bioavailability and an average maximum plasma concentration (C_{max}) of 0.89 (μ g/mL)

with a half-life ($t_{1/2}$) of 8.6 h in male ICR mice (Figure S8; PK study). We then orally administered SB1501 (10 mg/kg) to *db/db* mice daily for 5 weeks. For the control groups, rosiglitazone (15 mg/kg) and vehicle were orally administered in parallel.^[54] As shown in Figure 5a, bodyweight profiles showed significant weight-loss effects in the SB1501-treated group. The SB1501-treated group started to show significant weight-loss from day 27, resulting in an average bodyweight-loss of 5.2 g at the end of 5-weeks of SB1501 administration without significant change in the food intake (Figure 5b, c). In contrast, the vehicle- and rosiglitazone-treated groups showed weight-increases of 2.5 g and 11.6 g, respectively (Figure 5b). We observed significant weight-loss in epicardial white adipose tissue (EWAT) and marginal loss in brown adipose tissue (BAT) upon SB1501 treatment (Figure 5d).

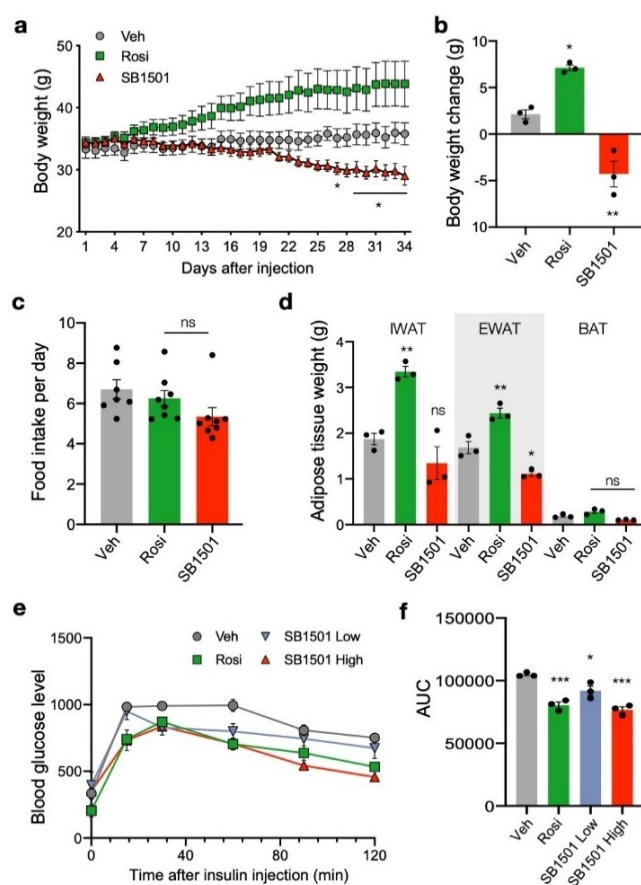


Figure 5. Improvement of metabolic profiles in a *db/db* mouse model after SB1501 administration. a) Monitoring body weight in *db/db* mice from day 1. $N=3$ for each group. b) Bodyweight change on day 34. c) Food intake per day in *db/db* mice. Food intake of each group was measured 8 times between day 20 and day 30, and averaged ($n=3$). Each dot represents an average food intake per day per group. d) Measurement of adipose tissue weight on day 34. IWAT: inguinal white adipose tissue; EWAT: epicardial white adipose tissue; BAT: brown adipose tissue. e) Glucose tolerance tests (GTTs) in *db/db* mice after administration of vehicle (Veh), rosiglitazone (Rosi, 15 mg/kg), or SB1501 (low: 10 mg/kg, high: 20 mg/kg) for 34 days. f) Quantification of the area under the curve (AUC) for the GTTs. All data are presented as mean \pm SEM; * $p < 0.05$, ** $p < 0.01$, *** $p < 0.001$ followed by one-way Dunnett's test. ns: not statistically significant.

Insulin resistance is a major metabolic characteristic of obesity and acts as a major factor in the pathogenesis of many obesity-related diseases, including type 2 diabetes.^[55] Therefore, anti-obesity therapeutics could exhibit beneficial effects on obesity-induced insulin resistance. To assess the effect of SB1501 on insulin resistance, we performed glucose tolerance tests (GTTs) on day 34 of treatment. Oral administration of 10 mg/kg (low) and 20 mg/kg (high) SB1501 exhibited a significant reduction in blood glucose level compared to the vehicle-treated group (Figure 5e). Accordingly, the net AUC was significantly reduced in the SB1501-treated group (Figure 5f). Moreover, the SB1501-treated group with a high dosage (20 mg/kg) ameliorated glucose tolerance to a level similar to that of rosiglitazone (Figure 5f). Together, SB1501 reduced adipose tissue mass and bodyweight while improving glucose tolerance in the *db/db* mouse model. These data suggest that SB1501 has therapeutic potential as an anti-obesity agent for the treatment of obesity and obesity-related insulin resistance.

SB1501 induces a browning process in IWAT and BAT

Finally, we analyzed the phenotypic changes in adipose tissues upon SB1501 treatment. Histological analysis of adipose tissues showed reduced LD sizes in both inguinal white adipose tissue (IWAT) and BAT in the SB1501-treated group compared to the vehicle- and rosiglitazone-treated groups (Figure 6a). In contrast, the rosiglitazone-treated group showed an increase in LD sizes in adipose tissues along with weight-increase (Figure 6a). Immunofluorescence imaging showed the upregulated expression of PGC-1 α and UCP1 in both adipose tissues along with reduced LD sizes (Figure 6b, c). Of note, the induction of UCP1 in IWAT increases their thermogenic capacity by dissipating fatty acids as heat, which is called the process of browning of IWAT.^[56] IWAT and BAT are metabolically active and mainly utilize lipids driven by upregulation of UCP1.^[57] In addition, the formation of small multilocular LDs is a representative phenotype of the browning process.^[58] These data suggest that SB1501 induces thermogenesis of adipose tissues through upregulation of the PGC-1 α -UCP1 regulatory axis, thereby reducing fat accumulation. We further analyzed the gene expression alterations in both adipose tissues. As expected, SB1501 significantly increased the mRNA levels of *Pgc-1 α* and

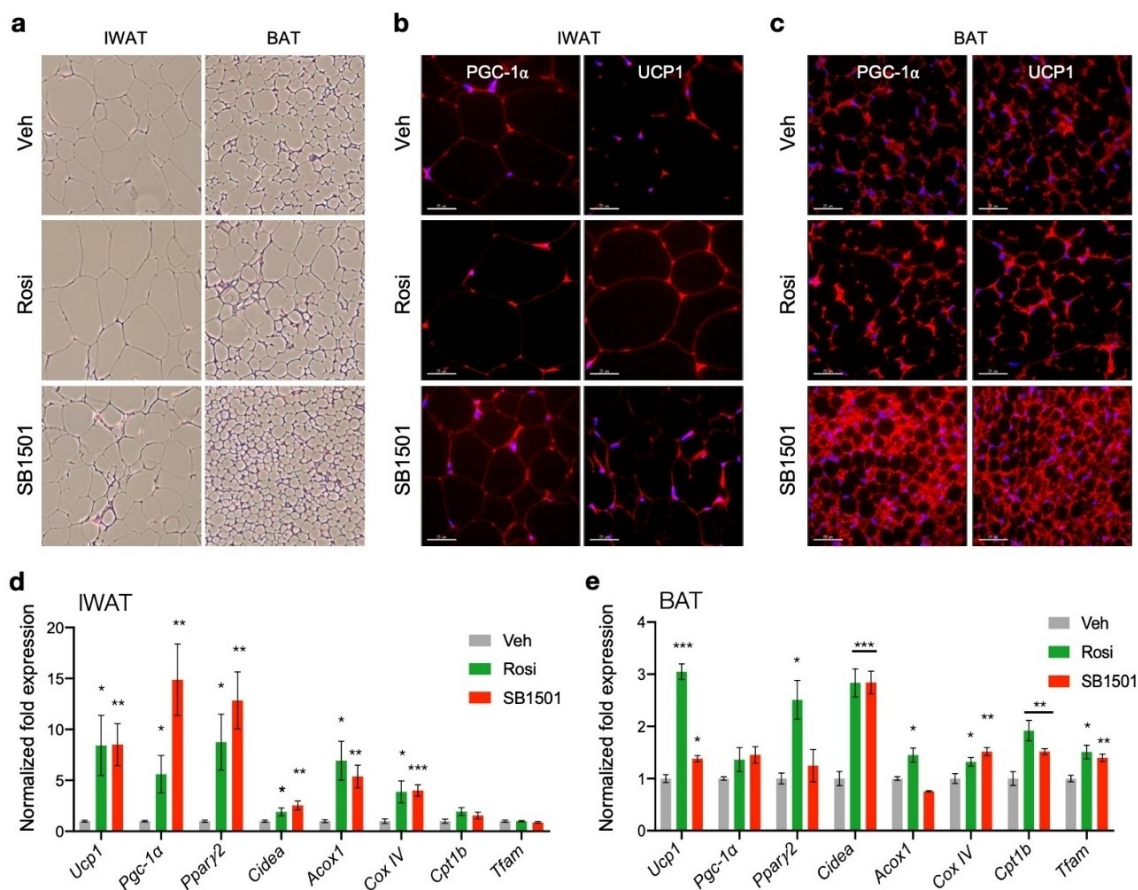


Figure 6. Changes in adipose tissue morphology and protein/mRNA expression in a *db/db* mouse model. a) Changes in adipose tissue morphology were monitored by H&E staining. b), c) Representative immunofluorescence images of adipose tissues stained with PGC-1 α and UCP1. Scale bars: 25 μ m. d), e) Quantitative analysis of mRNA expression in adipose tissues. Fold expressions of each gene were normalized to the vehicle-treated group. All data are presented as mean \pm SEM; * p < 0.05, ** p < 0.01, *** p < 0.001 followed by one-way Dunnett's test.

Ucp1 in IWAT (Figure 6d). Along with the upregulation of the brown adipocyte marker (*Cidea*), the genes for mitochondrial biogenesis and (*Cox IV*) and FAO (*Acox1* and *Cpt1b*) were increased in IWAT. *Cox IV* and *Cidea* are also known as the thermoregulatory gene. In BAT, we observed significant increases in the mRNA level of *Ucp1* in the SB1501-treated group; however, *Pgc-1 α* was not significantly perturbed (Figure 6e). Nonetheless, increases in the expression levels of genes regulating mitochondrial biogenesis and FAO in BAT were evident. We also observed that SB1501 reduces fat accumulation and upregulates the PGC-1 α signaling pathway in liver tissue (Figure S9). These data collectively show that SB1501 reduces fat accumulation in the multiple key metabolic tissues, including liver and adipose tissues, via perturbing the PGC-1 α -UCP1 signaling pathway.

Conclusion

Obesity is defined as a state of increased body weight, and chronic imbalance between energy intake and consumption is the main driver of obesity. Current treatment strategies for obesity predominantly focus on decreased energy intake and preventing the absorption of food. Appetite suppressants, such as phentermine, phendimetrazine, diethylpropion, and mazindol, cause a decrease in appetite by increasing the level of neurotransmitters that control hunger and fullness within the central nervous system.^[59] Besides, orlistat is a well-known prescribed obesity medication that suppresses lipase activities in the stomach and small intestine and blocks the absorption of TGs into fatty acids, which are absorbed into the intestinal tract, thereby showing a weight-loss effect.^[60] However, current anti-obesity agents (appetite suppressors and lipase inhibitors) have limited effectiveness and undesirable side effects, including insomnia, dizziness, headaches, vomiting, and oily bowel movements.^[61] Therefore, many anti-obesity therapeutics targeting different mechanisms are currently under investigation.^[62,63] Mitochondria are the main organelles for energy production, and promoting mitochondrial activity is currently used in the anti-obesity approach.^[64] However, small molecules targeting mitochondria remain challenging due to complex mechanisms, and only a few have anti-obesity efficacy with a suitable therapeutic window.

In this study, our research focused on enhancing cellular energy expenditure as an alternative strategy for developing a new anti-obesity agent. We aimed to discover a novel bioactive compound that reduces cellular LD accumulation. For the primary screening, we performed image-based high-throughput screening to monitor cellular LDs with fluorogenic LD bioprobe (SF44) in HeLa cells. Among 3,000 small molecules from an in-house pDOS library, we discovered hit compound **8** containing benzopyran-substituted 1,2,3-triazole core skeleton, which reduces cellular LDs by 67% without cytotoxic effect. Through the systematic SAR study, we discovered the lead compound **12**, namely SB1501, containing an electron-donating methoxy substituent at the *ortho* position of the phenyl group. SB1501 afforded the best LD-reducing efficacy with a twofold higher

EC₅₀ value in HeLa cells. We also demonstrated the LD-reducing effect of SB1501 in differentiating 3T3-L1 adipocytes. Interestingly, SB1501 reduced fat accumulation of 3T3-L1 adipocytes in a treatment time-dependent manner and showed better efficacy under treatment at the late stage of differentiation. In the process of revealing the SB1501's mechanism of action, we identified that the reduction of cellular LD accumulation by SB1501 is mainly associated with the perturbation of mitochondrial biogenesis and FAO. Mitochondrial FAO uses fatty acids as a cellular energy source and is regarded as a potential therapeutic target for obesity and obesity-related diseases. Long-term treatment of SB1501 in differentiating 3T3-L1 adipocytes upregulated the mRNA and protein expression of PGC-1 α and its downstream proteins, mainly involved in mitochondria biogenesis (PPAR α and TFAM) and FAO (UCP1, CPT1, CD36, and LPL). Consistent with those data, SB1501 increased both mitochondrial mass and maximal respiration. In addition, we observed an increase in mitochondrial fusion, consistent with the previously reported correlation between mitochondrial fusion and cellular fat reduction.^[65] Together, our data show that SB1501 reduces cellular fat accumulation by elevating mitochondrial biogenesis and FAO via the PGC-1 α -UCP1 signaling pathway.

We then demonstrated the therapeutic potential of SB1501 as an anti-obesity agent in the *db/db* mouse model. Oral administration of SB1501 significantly reduces body weight, compared to the vehicle-treated group. In addition to its weight-loss effect, SB1501 improved glucose tolerance, which is related to obesity-induced insulin resistance. Histopathological analysis of the adipose tissues also revealed that the treatment of SB1501 notably decreased the size of LDs in both IWAT and BAT, along with the formation of multiple small LDs in IWAT. The size and fat accumulation of LDs in IWAT and BAT are strongly linked to the induction of UCP1-mediated thermogenesis, which is primarily regulated by PGC-1 α . Treatment of SB1501 enhanced the mRNA and protein expression of PGC-1 α and UCP1 in adipose tissues, consistent with the *in vitro* studies in 3T3-L1 adipocytes. These data show that SB1501 upregulates UCP1, which dissipates energy as heat and plays a key role in the thermogenesis of mitochondria, resulting in increased FAO and reduced fat accumulation in adipose tissues. Furthermore, SB1501 significantly increased the mRNA expression levels of thermogenesis-related genes and brown adipocyte markers, including *UCP1*, *PGC-1 α* , *Cidea*, and *Cox IV* in IWAT, which suggests that SB1501 upregulates UCP1-mediated thermogenesis and induces browning process in IWAT. Collectively, we found that SB1501 showed an anti-obesity effect by activating adipose tissues via the upregulation of PGC-1 α and UCP1 as well as beneficial effects on liver fat accumulation in a *db/db* mouse model. At present, it is unclear whether SB1501 exhibited direct pharmacological effects in the liver or its LD-reducing effect in adipose tissues results in a reduction of ectopic fats in the liver. Nevertheless, our data show that SB1501 has the potential to improve obesity-induced systemic insulin resistance *in vivo*.

In conclusion, our study demonstrated that SB1501 has the potential as an anti-obesity agent. Our findings showed that

SB1501 improves obesity and obesity-induced insulin resistance *in vivo*. However, it still remains unclear what is the molecular target of SB1501. To understand its exact mechanism of action, we pursued the target identification of SB1501 with both a photoaffinity-based approach using FITGE^[66,67] and a label-free approach using thermal stability shift, namely TS-FITGE,^[68,69] but we haven't yet revealed the exclusive target proteins of SB1501, probably due to its low efficacy, tight SAR, and complex mechanism associated with multiple target proteins. The extensive target identification and validation of SB1501 are currently ongoing, and these results will be reported in due course.

Experimental Section

Cell lines. HeLa human cervical cancer cells and 3T3-L1 cells (mouse embryonic fibroblasts) were obtained from American Type Culture Collection. HeLa cells were maintained in RPMI medium containing 10% fetal bovine serum (FBS) and 1% antibiotic-antimycotic solution [GIBCO] at 37 °C in an atmosphere of 5% CO₂. 3T3-L1 cells were maintained in Dulbecco's modified Eagle's medium (DMEM) containing 10% heat-inactivated bovine calf serum (BCS) [GIBCO] and 1% antibiotic-antimycotic solution at 37 °C in an atmosphere of 5% CO₂.

Animal administration. Ten-week-old C57BLKS/J-*Lepr^{db}/Lepr^{db}* (*db/db*) male mice were obtained from Central Lab Animal Inc. (Seoul, Korea) and were housed in 12-h light/12-h dark cycles. Once they were 11 weeks of age, rosiglitazone (oral gavage, 15 mg/kg/day) and SB1501 (oral gavage, 10 and 20 mg/kg/day) were administered for 5 weeks. All animal experiments were performed in accordance with the research guidelines of the Seoul National University Institutional Animal Care and Use Committee.

3T3-L1 differentiation. 3T3-L1 preadipocyte cells were seeded on culture plates and incubated for 2 days at 37 °C in an atmosphere of 5% CO₂. After reaching 100% confluence, differentiation was induced by treating the cells with 1 μM dexamethasone, 10 μM rosiglitazone, and 5 μg/mL insulin in DMEM media containing 10% FBS for 2 days. Cells were maintained for 8 days by exchanging with fresh DMEM containing 10% FBS and 5 μg/mL insulin every 2 days.

Pharmacokinetics study. The following procedure obtained pharmacokinetic data. We tested two different routes of administration: intravenous (iv) injection at a concentration of 10 mg/kg (*n* = 1) and oral treatment at a dose of 10 and 20 mg/kg in ICR male mice (*n* = 2). SB1501 was prepared as a solution (DMSO, PEG400, and distilled water at 5:47:50, v/v/v %). In oral treatment, we obtained blood samples at 30 min, 1, 2, 4, 8, and 24 h after oral administration. In the case of iv injection, blood samples were taken at 5 min, 30 min, 1 h, 2 h, 4 h, 8 h, and 24 h after injection. After the centrifugation of plasma for purification, the concentration of SB1501 was analyzed using Agilent 6460 LC/MS/MS system [Agilent] using electron spray ionization. Pharmacokinetic parameters were obtained after the analysis of the plasma concentration–time plot with WinNonlin software [Pharsight].

Image-based high-throughput screening. HeLa cells were cultured on black 96-well plates for 1 day. Small molecules (10 μM) were added to the designated wells using a pin tool and incubated for 24 h. Oleic acid stock (100 mM) was prepared in isopropanol, and freshly dissolved to 10 mM in DMSO before use. Oleic acid (5 μM) and serum-free media were used as positive/negative controls. After exchanging with fresh medium, SF44 (5 μM) and Hoechst

33342 [Thermo Scientific] were added to individual wells. After 30 min incubation at 37 °C, without washing, fluorescence images of each well were acquired with InCell Analyzer 2000 [GE Healthcare]. Fluorescence images were captured using excitation/emission filters at CFP/Cy3 channels for SF44 and DAPI channel for Hoechst 33342. Fluorescence intensities were analyzed using the InCell Analyzer 1000 workstation 3.6 program [GE Healthcare]. Hit compounds reducing cellular LD organelle count were identified by calculating relative LD organelle count [%] for each well compared to the DMSO control well. In parallel, cell viability screening was performed to assess the cytotoxicity of each compound with WST assay kit [DoGenBio].

High-resolution imaging of LDs in 3T3-L1 adipocytes. 3T3-L1 preadipocytes were seeded on glass-bottom confocal dishes [Corning]. After reaching 100% confluence, cells were differentiated as described above. During the differentiation, cells were treated with SB1501 (40 μM) at different duration after the induction of differentiation while maintaining the cells with fresh DMEM containing 10% FBS and 5 μg/mL insulin. After 8 days, cells were stained with SF44 (20 μM) in DMEM containing 10% FBS and 5 μg/mL insulin for 30 min. After washing with phosphate-buffered saline (PBS) twice, DMEM containing 10% FBS and 5 μg/mL insulin was added for live-cell imaging. Fluorescence microscopy imaging was performed using the DeltaVision imaging system equipped with 60× objective lenses of Olympus IX-71 inverted microscope under 5% CO₂ at 37 °C. Every single LD within a cell was identified from the fluorescence images, then the mean area and fluorescence intensity were analyzed for the quantitative analysis of images using InCell Developer Toolbox v1.9.3. [GE Healthcare].

Quantitative reverse transcription PCR (qRT-PCR). 3T3-L1 cells were differentiated as described above. During the differentiation, cells were treated with 40 μM of SB1501 for 8 days while maintaining the cells with fresh DMEM containing 10% FBS and 5 μg/mL insulin. After 8 days, total RNA was isolated using RNA isolation kit [Qiagen]. Total RNA of adipose tissues were also isolated as described above. cDNA was synthesized using a reverse transcriptase kit and oligo(dT) primer according to the manufacturer's instruction [Bioneer]. Quantitative real-time PCR was performed with cDNA, primers, and SYBR Green [Kapa Biosystems]. The Applied Biosystems™ StepOnePlus real-time PCR system was used for qRT-PCR. All the primers for qRT-PCR were obtained from Bioneer.

Western blot analysis. 3T3-L1 cells were differentiated as described above. During the differentiation, cells were treated with 40 μM of SB1501 for 8 days while maintaining the cells with fresh DMEM containing 10% FBS and 5 μg/mL insulin. After 8 days, cell lysates were obtained by RIPA buffer [Cell Signaling Technology] containing 1× protease inhibitor cocktail [Roche]. The proteome was analyzed by SDS-PAGE and transferred into the PVDF membrane. After blocking with 2% BSA in Tris-buffered saline containing Tween 20 (TBST) for 1 h, membranes were treated with the desired primary antibody (1:1000 in 1% BSA-TBST) overnight at 4 °C. After washing with TBST 3 times, membranes were exposed to HRP-conjugated secondary antibody (1:2000 in 1% BSA-TBST) for 1 h at room temperature and developed by ECL Prime [GE Healthcare]. Chemiluminescent signal was scanned by ChemiDoc™ MP imaging system [BioRad].

Immunofluorescence imaging of 3T3-L1 cells. 3T3-L1 preadipocytes were seeded on glass-bottom dishes. After reaching 100% confluence, cells were differentiated as described above. During the differentiation, cells were treated with 40 μM of SB1501 for 8 days while maintained in fresh DMEM containing 10% FBS and 5 μg/mL insulin. After 8 days, cells were stained with Mitotracker Red (200 nM) in DMEM containing 10% FBS for 30 min. After washing

with phosphate-buffered saline (PBS), cells were incubated with fixation buffer (3.7% paraformaldehyde in PBS) for 15 min and permeabilization buffer (0.1% TritonX-100 in PBS) for 10 min. After blocking the cells with 4% BSA in PBS for 1 h at room temperature, the anti-UCP1 antibody (1:200 in 1% BSA-PBS) was incubated overnight at 4 °C. After washing with PBS three times, cells were incubated with FITC-conjugated secondary antibody (1:200 in 1% BSA-PBS) for 2 h at room temperature. After washing 5 times with PBS, the nucleus was stained with Hoechst 33342 and washed out. Fluorescence microscopy imaging was performed using the DeltaVision imaging system equipped with 60× objective lenses of Olympus IX-71 inverted microscope. The temperature was maintained at 23 °C.

Lipolysis assay. 3T3-L1 preadipocytes were seeded on 12-well plates [Nunc]. After reaching 100% confluence, cells were differentiated as described above. At day 8, cells were washed with lipolysis wash buffer and incubated with lipolysis assay buffer containing isoproterenol (ISO, 100 nM) for 2 h at 37 °C in an atmosphere of 5% CO₂. After 2 h, lipolysis assay buffers were harvested into 1.5 mL ep-tube and mixed the lipolysis reaction mixture containing glycerol probe and glycerol enzyme mix. A lipolysis assay was performed with Lipolysis assay kit [Abcam] according to the manufacturer's instruction. BCA protein assay [ThermoFisher Scientific] was performed to measure the protein concentration of the cell lysates. Absorbance values obtained from lipolysis assay were normalized with a lysate protein concentration of each sample.

Quantification of triglyceride concentration. 3T3-L1 cells were differentiated as described above. During the differentiation, cells were treated with 40 μM of SB1501 for 8 days while maintained in fresh DMEM containing 10% FBS and 5 μg/mL insulin. After 8 days, cells were homogenized with 5% NP-40 in ddH₂O. Triglyceride concentration within the homogenized cells was measured with Triglyceride Quantification Assay Kit [Abcam] according to the manufacturer's instruction.

Quantification of mitochondrial DNA. 3T3-L1 cells were differentiated as described above. During the differentiation, cells were treated with 40 μM of SB1501 for 8 days while maintained in fresh DMEM containing 10% FBS and 5 μg/mL insulin. After 8 days, genomic DNA was prepared with a DNA prep kit [Qiagen] according to the manufacturer's instruction. 10 ng of gDNA was mixed with a qPCR reaction mixture containing 1× KAPA SYBR FAST qPCR Master Mix, 200 nM of forward/reverse primers for 16S rRNA, or hexokinase 2 for a final volume of 20 μL. The PCR temperature cycling was used; initial denaturing at 95 °C for 1 min, followed by 40 cycles of denaturing at 95 °C for 15 s, and extension at 60 °C for 1 min. The copy number of 16S rRNA was normalized by the copy number of hexokinase 2.

Quantitative analysis mitochondrial network in 3T3-L1 adipocytes. 3T3-L1 preadipocytes were seeded on glass-bottom confocal dishes. After reaching 100% confluence, cells were differentiated as described above. During the differentiation, cells were treated with 40 μM of SB1501 for 8 days while maintaining the cells with fresh DMEM containing 10% FBS and 5 μg/mL insulin. After 8 days, cells were stained with MitoTracker Deep Red (200 nM), SF44 (20 μM), and Hoechst 33342 (2 μg/mL) in DMEM containing 10% FBS and 5 μg/mL insulin for 30 min. Carbonyl cyanide *m*-chlorophenylhydrazone (CCCP) was treated for 2 h on day 8. After washing with PBS twice, DMEM containing 10% FBS and 5 μg/mL insulin was added for live-cell imaging. Fluorescence microscopy imaging was performed using the DeltaVision imaging system equipped with 60× objective lenses of Olympus IX-71 inverted microscope under 5% CO₂ at 37 °C. Quantification of the mitochondrial network was performed with 3D Object Counter of Image J software.

Measurement of oxygen consumption rate. The oxygen consumption rate (OCR) of 3T3-L1 adipocytes was measured using a Seahorse XFe24 extracellular flux analyzer [Agilent] according to the manufacturer's protocols. Briefly, 3T3-L1 cells were seeded on XF24 cell culture microplates and differentiated as described above in the presence or absence of SB1501 (40 μM). To measure the mitochondrial respiration, 1.5 μM of oligomycin, 0.5 μM of FCCP (carbonyl cyanide-*p*-trifluoromethoxy-phenylhydrazone), and 0.5 μM of rotenone/antimycin A were added through the injection ports. During Seahorse analysis, 5 μg/mL insulin was added to the assay media. BCA protein assay was performed to measure the protein concentration of cell lysates. Data were normalized with a lysate protein concentration of each sample.

Glucose tolerance tests. For the glucose tolerance tests (GTTs), overnight (16 h) fasted *db/db* mice were orally injected with glucose (1 g/kg, 20% glucose solution). Blood samples were drawn at 15, 30, 60, 90, and 120 min after glucose injection by taking 3 μL of blood from the tip of the tail vein.

Immunohistochemistry of adipose tissues. The adipose tissues were isolated from mice, fixed in 4% paraformaldehyde, and embedded in a paraffin block. The paraffin blocks were trimmed (5-μm-thick) and mounted onto a glass slide. The tissue sections were dewaxed in xylene and rehydrated in a graded series of ethanol solutions (100, 90, 80, and 70%). For antigen retrieval, the slides were incubated in boiling sodium citrate buffer (10 mM, pH 6.0) for 30 min. The antigen retrieval step was skipped for slides stained with hematoxylin and eosin. After blocking the slices with 5% horse serum, sections were stained with primary antibodies against PGC-1α (sc-13067; Santa Cruz Biotechnology) and UCP1 (ab10983; Abcam). Secondary staining with anti-rabbit Alexa Fluor 594 goat antibody (A32740; Invitrogen) was followed. The sections were counterstained with hematoxylin and eosin dye. Fluorescence microscopy imaging was performed using the DeltaVision imaging system equipped with 60× objective lenses of Olympus IX-71 inverted microscope. The temperature was maintained at 23 °C.

Statistical analysis. The results are shown as mean ± SD for *in vitro* studies and SEM for *in vivo* studies. The unpaired student's *t*-test and one-way Dunnett's test were performed by GraphPad Prism8. *p* values of <0.05 were considered significant.

Author Contributions

A.J., M.K., and S.B.P. conceived the idea and designed the research outline. M.K. designed and synthesized all compounds. A.J., J.H., and H.N. executed the phenotypic screening, bioimaging, immunohistochemistry protocol, and western blot. J.-I.K., I.J.H., and J.B.K. designed and performed all animal experiments. A.J., M.K., and S.B.P. wrote the manuscript. All authors contributed to the discussion and approved the final version of this manuscript.

Acknowledgements

This work was supported by National Creative Research Initiative Grants (2014R1A3A2030423 to S.B.P.; 2020R1A3B2078617 to J.B.K.) and the Bio & Medical Technology Development Program (2012M3A9C4048780 to S.B.P.) through the National Research Foundation of Korea (NRF) funded by the Korean Government (Ministry of Science & ICT). A.J., M.K., and H.N. are grateful to the

BK21 Fellowship Program. J.H. is grateful to the Fostering Core Leaders of the Future Basic Science Program/Global Ph.D. Fellowship Program (NRF-2016H1A2A19 07084).

Conflict of Interest

The authors declare no conflict of interest.

Keywords: lipid droplets · metabolic diseases · obesity · PGC-1alpha-UCP1 · phenotype-based drug discovery

- [1] S. E. Kahn, R. L. Hull, K. M. Utzschneider, *Nature* **2006**, *444*, 840–846.
- [2] P. Kopelman, *Obes. Rev.* **2007**, *8 Suppl 1*, 13–17.
- [3] J. E. Hall, J. M. do Carmo, A. A. da Silva, Z. Wang, M. E. Hall, *Nat. Rev. Nephrol.* **2019**, *15*, 367–385.
- [4] S. Verma, M. E. Hussain, *Diabetes Metab. Syndr. Obes.* **2017**, *11*, 73–79.
- [5] G. B. D. O. Collaborators, A. Afshin, M. H. Forouzanfar, M. B. Reitsma, P. Sur, K. Estep, A. Lee, L. Marczak, A. H. Mokdad, M. Moradi-Lakeh, M. Naghavi, et al., *N. Engl. J. Med.* **2017**, *377*, 13–27.
- [6] M. Glandt, I. Raz, *J. Obes.* **2011**, *2011*, 636181.
- [7] A. Elangovan, R. Shah, Z. L. Smith, *Obes. Surg.* **2020**.
- [8] S. Henness, C. M. Perry, *Drugs* **2006**, *66*, 1625–1656.
- [9] D. K. Patel, F. C. Stanford, *Postgrad. Med.* **2018**, *130*, 173–182.
- [10] I. J. Onakpoya, C. J. Heneghan, J. K. Aronson, *BMC Med.* **2016**, *14*, 191.
- [11] D. Serra, P. Mera, M. I. Malandrino, J. F. Mir, L. Herrero, *Antioxid. Redox Signaling* **2013**, *19*, 269–284.
- [12] E. S. Childress, S. J. Alexopoulos, K. L. Hoehn, W. L. Santos, *J. Med. Chem.* **2018**, *61*, 4641–4655.
- [13] M. Goldgof, C. Xiao, T. Chanturiya, W. Jou, O. Gavrilova, M. L. Reitman, *J. Biol. Chem.* **2014**, *289*, 19341–19350.
- [14] U. S. Eggert, *Nat. Chem. Biol.* **2013**, *9*, 206–209.
- [15] D. C. Swinney, *Clin. Pharmacol. Ther.* **2013**, *93*, 299–301.
- [16] E. Kim, S. Lee, S. B. Park, *Chem. Commun.* **2012**, *48*, 2331–2333.
- [17] M. Konige, H. Wang, C. Sztalryd, *Biochim. Biophys. Acta.* **2014**, *1842*, 393–401.
- [18] J. J. Fuster, N. Ouchi, N. Gokce, K. Walsh, *Circ. Res.* **2016**, *118*, 1786–1807.
- [19] S. Lee, E. Kim, S. B. Park, *Chem. Sci.* **2013**, *4*, 3282–3287.
- [20] M. Zhu, B. J. Lim, M. Koh, S. B. Park, *ACS Comb. Sci.* **2012**, *14*, 124–134.
- [21] F. J. Ruiz-Ojeda, A. I. Ruperez, C. Gomez-Llorente, A. Gil, C. M. Aguilera, *Int. J. Mol. Sci.* **2016**, *17*, 1040.
- [22] S. R. Farmer, *Cell Metab.* **2006**, *4*, 263–273.
- [23] E. Ji, M. Y. Jung, J. H. Park, S. Kim, C. R. Seo, K. W. Park, E. K. Lee, C. H. Yeom, S. Lee, *Int. J. Obes. (Lond)* **2014**, *38*, 1035–1043.
- [24] Y. K. Park, J. Lee, V. S. Hong, J. S. Choi, T. Y. Lee, B. C. Jang, *PLoS One* **2014**, *9*, e109344.
- [25] N. A. Ducharme, P. E. Bickel, *Endocrinology* **2008**, *149*, 942–949.
- [26] M. A. Aon, N. Bhatt, S. C. Cortassa, *Front. Plant Physiol.* **2014**, *5*, 282.
- [27] N. Turner, C. R. Bruce, S. M. Beale, K. L. Hoehn, T. So, M. S. Rolph, G. J. Cooney, *Diabetes* **2007**, *56*, 2085–2092.
- [28] Y. Zhang, L. W. Castellani, C. J. Sinal, F. J. Gonzalez, P. A. Edwards, *Genes Dev.* **2004**, *18*, 157–169.
- [29] B. N. Finck, D. P. Kelly, *J. Clin. Invest.* **2006**, *116*, 615–622.
- [30] P. J. Fernandez-Marcos, J. Auwerx, *Am. J. Clin. Nutr.* **2011**, *93*, 884S–890.
- [31] C.-F. Cheng, H.-C. Ku, H. Lin, *Int. J. Mol. Sci.* **2018**, *19*, 3447.
- [32] H. P. Harding, Y. Zhang, S. Khersonsky, S. Marciniak, D. Scheuner, R. J. Kaufman, N. Javitt, Y. T. Chang, D. Ron, *Cell Metab.* **2005**, *2*, 361–371.
- [33] P. Keller, J. T. Petrie, P. De Rose, I. Gerin, W. S. Wright, S. H. Chiang, A. R. Nielsen, C. P. Fischer, B. K. Pedersen, O. A. MacDougald, *J. Biol. Chem.* **2008**, *283*, 14355–14365.
- [34] K. Makki, P. Froguel, I. Wolowczuk, *ISRN Inflamm.* **2013**, *2013*, 139239.
- [35] A. E. Achari, S. K. Jain, *Int. J. Mol. Sci.* **2017**, *18*, 1321.
- [36] M. Schweiger, T. O. Eichmann, U. Taschler, R. Zimmermann, R. Zechner, A. Lass, *Methods Enzymol.* **2014**, *538*, 171–193.
- [37] A. Yang, E. P. Mottillo, *Biochem. J.* **2020**, *477*, 985–1008.
- [38] P. Morigny, M. Houssier, E. Mouisel, D. Langin, *Biochimie* **2016**, *125*, 259–266.
- [39] M. Schweiger, M. Romauch, R. Schreiber, G. F. Grabner, S. Hutter, P. Kotzbeck, P. Benedikt, T. O. Eichmann, S. Yamada, O. Knittelfelder, C. Diwok, C. Doler, N. Mayer, W. De Cecco, R. Breinbauer, R. Zimmermann, R. Zechner, *Nat. Commun.* **2017**, *8*, 14859.
- [40] F. Zalatan, J. A. Krause, D. E. Blask, *Endocrinology* **2001**, *142*, 3783–3790.
- [41] N. Mayer, M. Schweiger, M. Romauch, G. F. Grabner, T. O. Eichmann, E. Fuchs, J. Ivkovic, C. Heier, I. Mrak, A. Lass, G. Hofler, C. Fledelius, R. Zechner, R. Zimmermann, R. Breinbauer, *Nat. Chem. Biol.* **2013**, *9*, 785–787.
- [42] M. E. Patti, S. Corvera, *Endocr. Rev.* **2010**, *31*, 364–395.
- [43] E. E. Blaak, D. P. van Aggel-Leijssen, A. J. Wagenmakers, W. H. Saris, M. A. van Baak, *Diabetes* **2000**, *49*, 2102–2107.
- [44] H. Zong, J. M. Ren, L. H. Young, M. Pypaert, J. Mu, M. J. Birnbaum, G. I. Shulman, *Proc. Natl. Acad. Sci. USA* **2002**, *99*, 15983–15987.
- [45] M. J. Betz, S. Enerbäck, *Nat. Rev. Endocrinol.* **2018**, *14*, 77–87.
- [46] D. G. Nicholls, *Biochim. Biophys. Acta.* **2006**, *1757*, 459–466.
- [47] K. Schneider, J. Valdez, J. Nguyen, M. Vawter, B. Galke, T. W. Kurtz, J. Y. Chan, *J. Biol. Chem.* **2016**, *291*, 7754–7766.
- [48] M. Liesa, O. S. Shirihai, *Cell Metab.* **2013**, *17*, 491–506.
- [49] T. Kita, H. Nishida, H. Shibata, S. Niimi, T. Higuti, N. Arakaki, *J. Biochem.* **2009**, *146*, 787–796.
- [50] P. H. Ducluzeau, M. Priou, M. Weitheimer, M. Flamment, L. Duluc, F. Iacobazi, R. Soleti, G. Simard, A. Durand, J. Rieusset, R. Andriantsitohaina, Y. Malthiery, *J. Physiol. Biochem.* **2011**, *67*, 285–296.
- [51] Q. Zheng, J. Lin, J. Huang, H. Zhang, R. Zhang, X. Zhang, C. Cao, C. Hambly, G. Qin, J. Yao, R. Song, Q. Jia, X. Wang, Y. Li, N. Zhang, Z. Piao, R. Ye, J. R. Speakman, H. Wang, Q. Zhou, Y. Wang, W. Jin, J. Zhao, *Proc. Natl. Acad. Sci. USA* **2017**, *114*, E9474–E9482.
- [52] H. Wang, M. Willershauser, A. Karlas, D. Gorpas, J. Reber, V. Ntziachristos, S. Maurer, T. Fromme, Y. Li, M. Klingenspor, *Mol. Metab.* **2019**, *20*, 14–27.
- [53] F. Shamsi, R. Xue, T. L. Huang, M. Lundh, Y. Liu, L. O. Leiria, M. D. Lynes, E. Kempf, C. H. Wang, S. Sugimoto, et al., *Nat. Commun.* **2020**, *11*, 1421.
- [54] P. Seale, H. M. Conroe, J. Estall, S. Kajimura, A. Frontini, J. Ishibashi, P. Cohen, S. Cinti, B. M. Spiegelman, *J. Clin. Invest.* **2011**, *121*, 96–105.
- [55] M. P. Czech, *Nat. Med.* **2017**, *23*, 804–814.
- [56] M. Harms, P. Seale, *Nat. Med.* **2013**, *19*, 1252–1263.
- [57] K. Ikeda, P. Maretich, S. Kajimura, *Trends Endocrinol. Metab.* **2018**, *29*, 191–200.
- [58] V. Peirce, S. Carobbio, A. Vidal-Puig, *Nature* **2014**, *510*, 76–83.
- [59] K. Suzuki, C. N. Jayasena, S. R. Bloom, *Exp. Diabetes Res.* **2012**, *2012*, 824305.
- [60] A. M. Heck, J. A. Yanovski, K. A. Calis, *Pharmacotherapy* **2000**, *20*, 270–279.
- [61] R. J. Rodgers, M. H. Tschop, J. P. Wilding, *Dis. Model. Mech.* **2012**, *5*, 621–626.
- [62] P. Flachs, M. Rossmeisl, O. Kuda, J. Kopecky, *Biochim. Biophys. Acta.* **2013**, *1837*, 986–1003.
- [63] J. Lee, J. M. Ellis, M. J. Wolfgang, *Cell Rep.* **2015**, *10*, 266–279.
- [64] J. A. Harper, K. Dickinson, M. D. Brand, *Obes. Rev.* **2001**, *2*, 255–265.
- [65] R. Putti, R. Sica, V. Migliaccio, L. Lionetti, *Front. Plant Physiol.* **2015**, *6*, 109.
- [66] J. Park, S. Oh, S. B. Park, *Angew. Chem. Int. Ed.* **2012**, *51*, 5447–5451; *Angew. Chem.* **2012**, *124*, 5543–5547.
- [67] S. Lee, Y. Nam, J. Y. Koo, D. Lim, J. Park, J. Ock, J. Kim, K. Suk, S. B. Park, *Nat. Chem. Biol.* **2014**, *10*, 1055–1060.
- [68] H. Park, J. Ha, J. Y. Koo, J. Park, S. B. Park, *Chem. Sci.* **2017**, *8*, 1127–1133.
- [69] H. Park, S. B. Park, *Chem. Sci.* **2019**, *10*, 3449–3458.

Manuscript received: January 25, 2021

Accepted manuscript online: February 3, 2021

Version of record online: March 10, 2021

Correction added on March 24, 2021, after first online publication: Assignment of author first and last names were corrected. Figure 3b was corrected as the 2nd & 6th entries of the x-axis were mislabeled. None of the minor corrections affect the scientific content and conclusions of the article.